Physica Scripta

PAPER

RECEIVED
26 September 2025

REVISED
5 November 2025

ACCEPTED FOR PUBLICATION
18 November 2025

PUBLISHED
28 November 2025

Abnormal performance of the Schottky barrier diodes extraction methods under bias dependent series resistance

Julio C Tinoco[1], **Rodolfo Garcia**[2] **and Andrea G Martinez-Lopez**[1,*]

[1] Micro and Nanotechnology Research Centre, Universidad Veracruzana, Blvd. Adolfo Ruíz Cortines 455, Costa Verde, 94294 Boca del Río, Ver., Mexico
[2] University Center UAEM Ecatepec, Universidad Autónoma del Estado de México, Ecatepec de Morelos 55020, Mexico
[*] Author to whom any correspondence should be addressed.

E-mail: andmartinez@uv.mx

Keywords: schottky barrier diodes, ideality factor, series resistance, extraction methods

Abstract

Schottky Barrier Diodes fabricated using nanostructured semiconductor materials have gained the attention of the community due to their potential novel applications as well as their use as circuit element. The electrical characterization of these kinds of devices usually gives ideality factor values greater than two and within a large dispersion. Different extraction methodologies have been developed based on the consideration that the diode parameters are constant. However, it has been found that the density-of-states into the semiconductor band gap produces a change of the semiconductor electron density as the applied voltage is increased, causing the presence of bias dependent series resistance, but its impact on the extraction procedures has not been properly addressed. Hence, numerical solution of the diode equation was performed with constant diode parameters and using bias dependent series resistance, three most used extraction methods were applied to analyse the possibility to properly estimate the diode parameters. It was found that extraction methods are no longer valid when diodes exhibit bias dependent parameters.

1. Introduction

Schottky barrier diodes (SBD) have been important devices for the industry due to their usefulness to semiconductor and interface characterization, circuital element applications or their potential as sensor devices [1, 2]. In recent years, SBD fabricated based on nanostructured semiconductors have gained attention for sensor applications and the possibility to support the development of flexible electronic systems [3–5]. Different semiconductor materials [6–9], synthesis and film deposition methods and temperatures [10–14], as well as metal electrodes [15–17] have been used for nanostructured diode fabrication. The electrical characterization is based on the thermionic emission theory, and the assessment of the diode parameters which are the metal-semiconductor barrier height (ϕ_b), the ideality factor (η), and series resistance (R_S). Table 1 summarizes the main nanostructured diode features for some devices previously reported [18–25], the diode parameters and the extraction methods used are indicated.

As can be observed in table 1, nanostructured SBD exhibits three main features: (i) low rectification ratios (I_{ON}/I_{OFF}) within a range of one and three orders of magnitude; (ii) relatively large series resistances; and (iii) ideality factor higher than 2.

However, table 1 also shows a high dispersion between reported values of η, from ~ 2 until higher than 10 [21, 25], but also it is possible to see high differences on the estimated values when different extraction methods are used [21, 22, 26]. Furthermore, it has been reported variation on the estimated ideality factor values with the device area [26], dependence with the applied bias [27], or even values smaller than one [28]. On the other hand, several reports also found ideality factor values very close to one [29–31].

Table 1. Summary of the SBD reported.

Semiconductor film	Morpho-logy	Metal electrode	Diode parameters extraction												Method	Reference
			η		ϕ_b (eV)		R_S(kΩ)		I_{ON}/I_{OFF}							
ZnO	Nanorods	Pd	8.2		0.66		—		44.22						a	[18]
ZnO	Nano-composite	Ag	5.26[a]		0.69[a]	0.68[b]	2.25[d]	2.27[e]	—						a,b	[19]
ZnO/GO 5%			5.21[a]		0.65[a]	0.64[b]	1.89[d]	1.89[e]	—							
ZnO/GO 10%			5.03[a]		0.62[a]	0.63[b]	1.56[d]	1.56[e]	—							
ZnO/GO 25%			4.64[a]		0.60[a]	0.62[b]	0.75[d]	0.75[e]	—							
ZnO @ Zn 0.2M	Nano-crystalline	Cu	3.01		0.69		—		4.92						a	[20]
ZnO @ Zn 0.5M			2.78		0.54		—		0.78							
ZnO @ Zn 0.8M			3.33		0.55		—		2.08							
ZnO @ Zn 1.0 M			3.22		0.60		—		2.01							
ZnO	Nano-particles	Pt	3.01[a]	7.49[b]	0.66[a]	0.41[b]	0.12[e]		$\sim 10^3$						a,b	[21]
ZnO:0.2%Sb		Al	6.45[a]	7.94[b]	0.70[a]	0.42[b]	21.57[e]		$< 10^3$							
ZnO:0.4%Sb		Al	10.98[a]	8.54[b]	0.68[a]	0.41[b]	14.66[e]		$< 10^3$							
ZnO	Nano-crystalline	Au	6.3[a]	3.12[b]	0.74[a]	0.77[b]	69.9[d]	24.6[e]	47						a,b	[22]
AZO			6.6[a]	2.63[b]	0.75[a]	0.80[b]	3.28[d]	5.63[e]	29							
ZnO	Nanorods	Cu 50nm	6.19[a]		0.7[a]		190[d]		—						a,b	[23]
		Cu 100nm	6.16[a]		0.66[a]		180[d]		—							
		Cu 150nm	5.08[a]		0.58[a]		50[d]		—							
		Cu 200nm	5.86[a]		0.53[a]		90[d]		—							
ZnO without bending	Poly-crystalline	Ag	2[a]	2.8[b]	0.7[b]	0.67[c]	0.008[d]	0.0063[c]	—						a,b,c	[24]
							0.006[e]									
ZnO with bending			3[a]	2.9[b]	0.68[b]	0.63[c]	0.0056[d]	0.0054[c]	—							
							0.0042[e]									
ZnO	—	Ag	1.64[a]	2.35[b]	0.85[a]		2.86[d]		3×10^6						a,b,c	[25]
					0.78[b]		2.64[e]									
					0.79[c]		1.13[c]									

[a] Idealized I–V.
[b] Cheung.
[c] Norde.
[d] Calculated from equation (4).
[e] Calculated from equation (5).

The theoretical η value considering thermionic emission is unity, thus, a different value can be considered as a kind of measure of the deviation from the ideal current—voltage (I–V) characteristic. Several explanations have been proposed to justify the η deviation from unity, the main are:

- Presence of barrier height inhomogeneity (BHI).
- Impact of series resistance.
- Existence of surface states at the semiconductor/metal interface.
- Presence of a nanometric interfacial dielectric layer.
- Influence of semiconductor defects.
- Presence of carrier recombination mechanisms.
- Contribution of additional conduction mechanisms.

However, the ideality factor for nanostructured semiconductors does not show a plain trend on the reported values, but neither the form how those explanations, usually considered, impact on η nor the degree of deviation introduced.

Furthermore, the traditional extraction methods have been developed considering that series resistance remains constant [32–35]. On the contrary, nanostructured semiconductors are characterized by the presence of a density of localized stated (DOS) into de semiconductor bandgap, and it has been shown that its impact

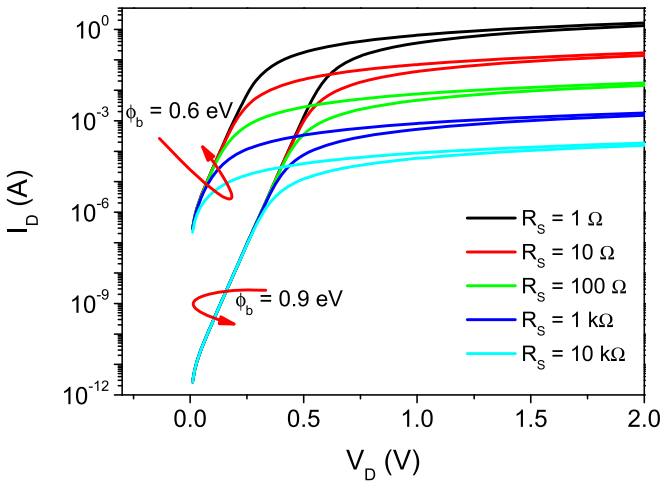

Figure 1. Current – voltage characteristics numerically calculated considering constant diode parameters and different values of the series resistance.

into the Schottky diode produce a bias dependent series resistance. Therefore, it is not clear whether the traditional extraction methods are able to accurately estimate the diode parameters particularly the ideality factor.

Therefore, in this contribution, it is analysed the usefulness of the three main used extraction methods by numerical solution of the diode equation, considering a constant as well as bias dependent series resistance. Additionally, experimental *I–V* characteristic of ZnO based diodes have been analysed to verify the extraction methodologies behaviour.

2. SBD extraction methods

As can be observed in table 1, the most used extraction procedures are idealized, i.e. without R_S, *I–V* plot, Cheung [32], and Norde function [33] methods. It is worth noticing that these methods were developed considering constant values of the diode parameters (ϕ_b, η and R_S). Hereafter, these methods are briefly described.

2.1. Idealized I–V plot extraction process

The ideal *I–V* characteristics of SBD is defined as:

$$I_D = AA^*T^2 \exp\left(-\frac{q\phi_b}{kT}\right)\left[\exp\left(\frac{qV_D}{\eta kT}\right) - 1\right] \tag{1}$$

where A is the device area, A^* is the Richardson constant, T is the device temperature, q is the electron charge, and k is the Boltzmann constant.

Considering the forward region and that $V_D \gg kT/q$, the ideality factor and barrier height can be determined as:

$$\eta = \frac{q}{kT}\cdot\frac{1}{\frac{d(\ln(I_D))}{dV_D}} = \frac{q}{kT}\cdot\frac{\Delta V_D}{\Delta(\ln(I_D))} \;\&\; \phi_b = \frac{kT}{q}\cdot\ln\left(\frac{AA^*T^2}{I_0}\right) \tag{2}$$

where I_0 is the diode current at $V_D = 0$ V.

Hence, the ideality factor can be determined from the inverse of the derivative of the $\ln(I_D)$ versus V_D, or from the inverse of the slope of the linear region in the semilogarithmic *I–V* characteristic. Regarding I_0 it can be found as the *y*-axis intercept of the linear region of the semilogarithmic *I–V* plot.

2.2. Cheung extraction method

The Cheung method [32] considers the presence of a series resistance; hence, the diode current is expressed as [32]:

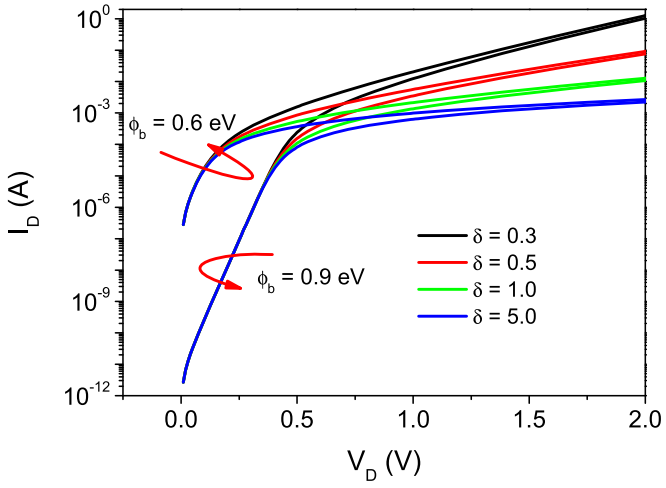

Figure 2. Current – voltage characteristics numerically calculated considering bias dependent series resistance and different values of δ.

$$I_D = AA^*T^2 \exp\left(-\frac{q\phi_b}{kT}\right)\left[\exp\left(\frac{q(V_D - I_D R_s)}{\eta kT}\right) - 1\right] \tag{3}$$

Also, the derivative of the $\ln(I_D)$ respect the forward bias is defined as:

$$\frac{dV_D}{d(ln(I_D))} = R_S I_D + \frac{kT}{q}\eta \tag{4}$$

Equation (4) has a linear dependence respect I_D, where the slope defines the series resistance, and the intercept is related with the ideality factor.

Moreover, the H function is defined as:

$$H = V - \frac{kT}{q}\eta \cdot \ln\left(\frac{I_D}{AA^*T^2}\right) = R_S I_D + \eta \cdot \phi_b \tag{5}$$

The H function also has a linear dependency with I_D, where the slope can be used to confirm the series resistance, and the intercept is related to the barrier height.

2.3. Norde function extraction method

This method determines the series resistance and the barrier height at forward bias from (3), and considering $V_D \gg kT/q$, based on the F function defined as [33]:

$$F = \frac{V_D}{2} - \frac{kT}{q} ln\left(\frac{I_D}{AA^*T^2}\right) \tag{6}$$

The F function, usually known as Norde´s function, exhibits a minimum in the F–V plot, where the F_0, V_0 and I_0 (through V_0) values can be found. Hence, the diode parameters can be estimated as:

$$R_S = \frac{kT}{qI_0} \;\&\; \phi_b = F_0 + \frac{V_0}{2} - \frac{kT}{q} \tag{7}$$

3. Theoretical *I*–*V* characteristic

The diode forward current was found by the numerical calculation of (3), considering different values of R_S from 1 Ωto 10 kΩ. A constant value of the ideality factor, fixed to unity, and two values of the barrier height, 0.6 and 0.9 eV, were used. Figure 1 shows the different I–V characteristics numerically obtained.

Additionally, in [26] was found that the density-of-states (DOS) into the semiconductor bandgap promotes an increment on the electron density into the semiconductor film, and as consequence, R_S is reduced, acquiring a dependence with the forward bias of the form:

$$R_S = R_0 \exp\left(-\frac{V_D}{\delta}\right) \tag{8}$$

where R_0 is the resistance at zero bias and δ is a fitting parameter.

Equation (3) but including bias dependent resistance as stated in (8) was also numerically solved with the same values for ϕ_b and η, a constant value of 1 kΩ for R_0 and different values of δ. Figure 2 shows the numerically calculated I–V characteristics.

Furthermore, the extraction methods shown in section 2 were applied with the aim of verifying the feasibility of these methods to estimate diode parameters.

4. Analysis of the extraction methods

The three extraction methods were applied to the first set of calculated I–V characteristics, i.e. with constant diode series resistance, figures 3(a)–(c) show key plots obtained for each method and the summary of the estimated values is presented in table 2.

Figure 3(a) shows the plot of the $\ln(I_D)$ versus V_D for both barrier height values used, for comparison the corresponding ideal current, with $R_S = 0\,\Omega$, is shown. As can be seen, for relatively large barriers the linear region is well defined, hence η and ϕ_b can be extracted using (2). However, the linear region is reduced as the resistance is increased, in the plot with 10 kΩ the useful extraction region is limited to the voltage range from about 50 mV to 300 mV. This limited range can compromise the accuracy of the estimated parameters. On the other hand, for relatively low barriers the linear region can be observed only for low resistances also in a voltage range limited to an extension of $\Delta V \sim 200$ mV for 1 Ω. For higher resistances the linear region is not shown. Therefore, as expected, the ideal procedure is limited to properly estimate the diode parameters, in particular when the device exhibits low barrier height and relatively high resistances, which is expected for nanostructured SBD as table 1 shows.

Figure 3(b) shows the corresponding plots used in the Cheung Method for $R_S = 10$ kΩ and $\phi_b = 0.9$ eV, and in the inset at 0.6 eV. As observed, both graphs exhibit a linear dependence as indicated in equations (4) and (5), therefore the three diode parameters can be properly estimated. It is worth noticing that the extension of both plots is the full bias range used, i.e. from 0 to 2.5 V, hence the Cheung method is not affected by constant series resistance into the range analysed.

Figure 3(c) shows the plot of the Norde function for both barrier heights used. As observed, the minimum is well defined and R_S and ϕ_b can be found using (7). Nonetheless, the precision on the determination of minimum (F_0, V_0) can be compromised as shown in the inset of figure 3(c), where more than one measured point can be very close each other. Hence the Norde method properly allows to determine the barrier height, but the resistance estimation starts to deviate from theoretical value for devices with large R_S and low barriers.

Also, the three extraction methods were applied to the second set of calculated I–V characteristics, i.e. considering a bias dependent series resistance. Figures 4(a)–(c) show the key plots for each method.

Figure 4(a) shows the $\ln(I_D)$ versus V_D plot for both barrier heights used, for comparison the corresponding ideal current is shown. For relatively large barriers, a linear region is observed, although in a limited bias range. On the contrary, for low barriers, linear region is not defined, therefore the method cannot be applied. In the inset it is shown the curve for $\delta = 5$, and $\phi_b = 0.6$ eV. As V_D is increased, the current increment is limited by the resistance, thus, into a very small bias range, it is possible to see several quasi-linear regions, each one with a specific slope and y-axis intercept, as red dashed lines depict. As V_D increases, the slope is reduced, while the intercept is increased. Therefore, according to (2), these changes imply that the estimated ideality factor is increased from 1 to 10, while the barrier height is reduced from 0.6 to 0.48 eV, in the regions indicated.

Figure 4(b) shows the plot of $\mathrm{d}V_D/\mathrm{dln}(I_D)$ versus I_D, for $\delta = 5$. As shown, there is not a linear behaviour, which implies that (4) is not valid. Similarly, to idealized method, it is possible to see several quasi-linear regions as the current increases, where the slope will be reduced and the intercept is increased. This implies that the estimated ideality factor will be increased from values of 1.1 to 19, correspondingly the resistance is reduced from 780 to 300 Ω which is out of the variation expected from (8) for the range of V_D used. As comparison the calculated curve for the corresponding constant resistance case, i.e. $\delta \to \infty$, is shown, it can be clearly seen that the resistance change produces the observed curve bending. Additionally, the difficulty of getting a reliable ideality factor value, implies that the H function cannot be calculated since the value of η is required in (5).

Figure 4(c) shows the plot of F versus V_D. for both barrier height values. Using the minimum, it is possible to estimate the barrier height values, in all cases the obtained values were 0.9 and 0.6 eV, respectively. On the other hand, a single resistance value can be estimated, and the resistance dependence on V_D cannot be obtained.

Therefore, the Cheung and Norde extraction methods allow to properly determine the diode parameters, for a wide range of resistances when such parameters are bias independent. However, as figures 4(a)–(c) show, when a bias dependent resistance is included, the extraction methods produce a fictitious increment on the ideality factor, and its value will change depending on the bias region and the voltage range (ΔV) used to perform the extraction. Therefore, it is not possible to develop a self-consistent comparison between the values

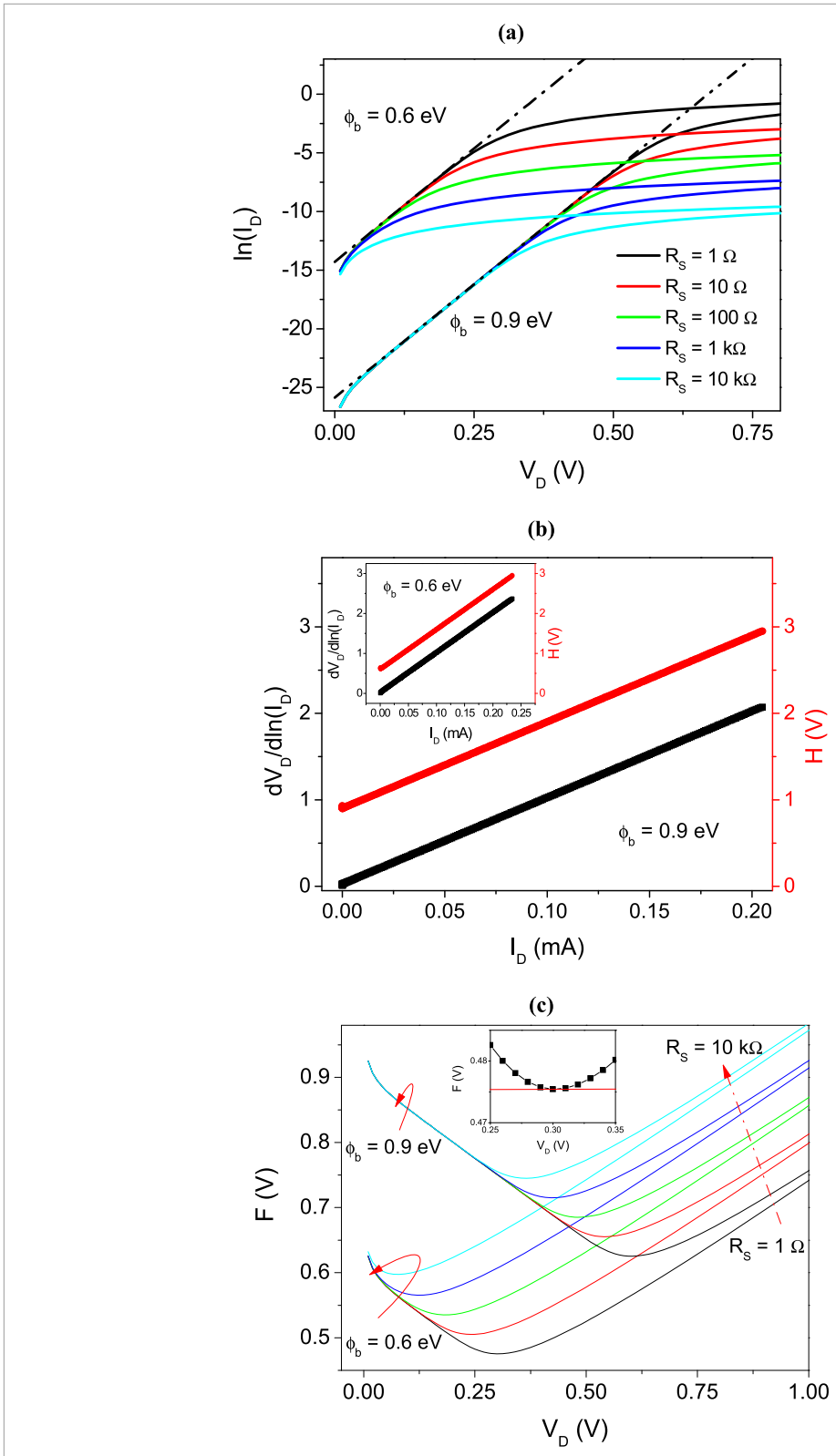

Figure 3. Extraction for numerical calculated $I-V$ characteristics with constant parameters. (a) $\ln(I_D)$ versus V_D plot for several R_S and both ϕ_b values used. (b) $dV_D/d\ln(I_D)$ and H versus I_D at $R_S = 10\ \text{k}\Omega$ and $\phi_b = 0.9$ eV. In the inset the corresponding plot for $\phi_b = 0.6$ eV is shown. (c) Norde function plot for the several R_S and both ϕ_b values used. In the inset a zoom in near the minimum for the curve corresponding to $R_S = 1\ \Omega$ and $\phi_b = 0.6$ eV is shown.

of the parameters, the extraction methods nor the features of the SBD processing. This behaviour of the extraction methods can contribute to the wide spread of reported values as table 1 shows.

In order to understand the performance of the extraction methods under bias dependent parameters, indicated as $\eta(V_D)$, $\phi_b(V_D)$ and $R_S(V_D)$, it is necessary to consider the equations (1) and (3).

Table 2. Summary of the SBD parameters estimated by the extraction methods for *I–V* numerically calculated using constant diode parameters.

R_S (Ω)	*I–V* characteristic calculated using $\eta = 1$ & $\phi_b = 0.6$ eV								*I–V* characteristic calculated using $\eta = 1$ & $\phi_b = 0.9$ eV							
	Idealized *I–V*		Cheung				Norde		Idealized *I–V*		Cheung				Norde	
	η	ϕ_b (eV)	η	ϕ_b (eV)	R_S[a] (Ω)	R_S[b] (Ω)	ϕ_b (eV)	R_S (Ω)	η	ϕ_b (eV)	η	ϕ_b (eV)	R_S[a] (Ω)	R_S[b] (Ω)	ϕ_b (eV)	R_S (Ω)
1	—	—	1	0.6	1	1	0.6	1	1	0.9	1	0.9	1	1	0.9	1
10	—	—	1	0.6	10	10	0.6	10	1	0.9	1	0.9	10	10	0.9	10
100	—	—	1	0.6	100	100	0.6	105	1	0.9	1	0.9	100	100	0.9	105
1000	—	—	1	0.6	1000	1000	0.6	1070	1	0.9	1	0.9	1000	1000	0.9	1060
10000	—	—	1	0.6	10000	10000	0.6	8000	1	0.9	1	0.9	10000	10000	0.9	10650

[a] Resistance calculated from (4).
[b] Resistance calculated from (5).

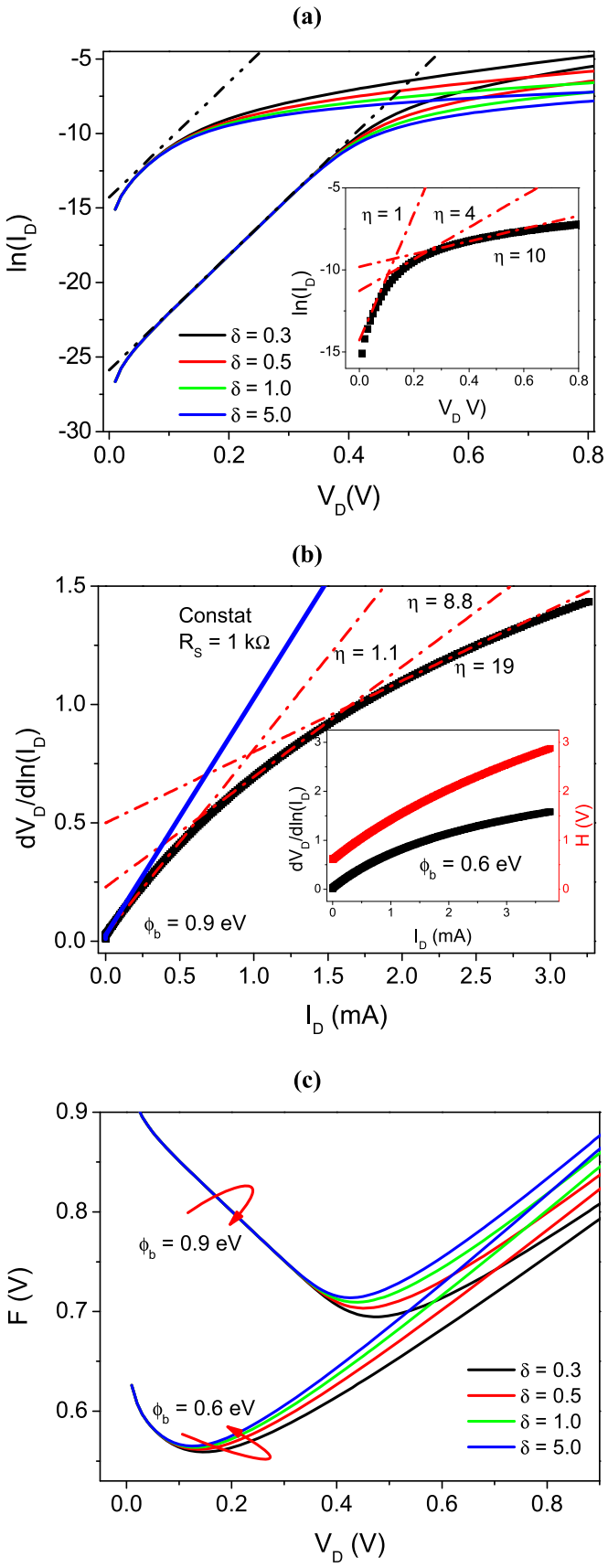

Figure 4. Extraction for numerical calculated $I-V$ characteristics with bias dependent resistance. (a) $\ln(I_D)$ versus V_D plot for several δ and both ϕ_b values. In the inset the curve for $\phi_b = 0.6$ eV and $\delta = 5$ is shown, straight lines for different quasi-linear regions and the η values are shown. (b) $dV_D/d\ln(I_D)$ versus I_D at $\phi_b = 0.9$ eV $\delta = 5$. In the inset the curve for $\phi_b = 0.6$ eV is shown, straight lines for different quasi-linear regions and the η values are shown. For comparison the plot for constant resistance is shown in blue line. (c) Norde function plot for the several δ and both ϕ_b values used.

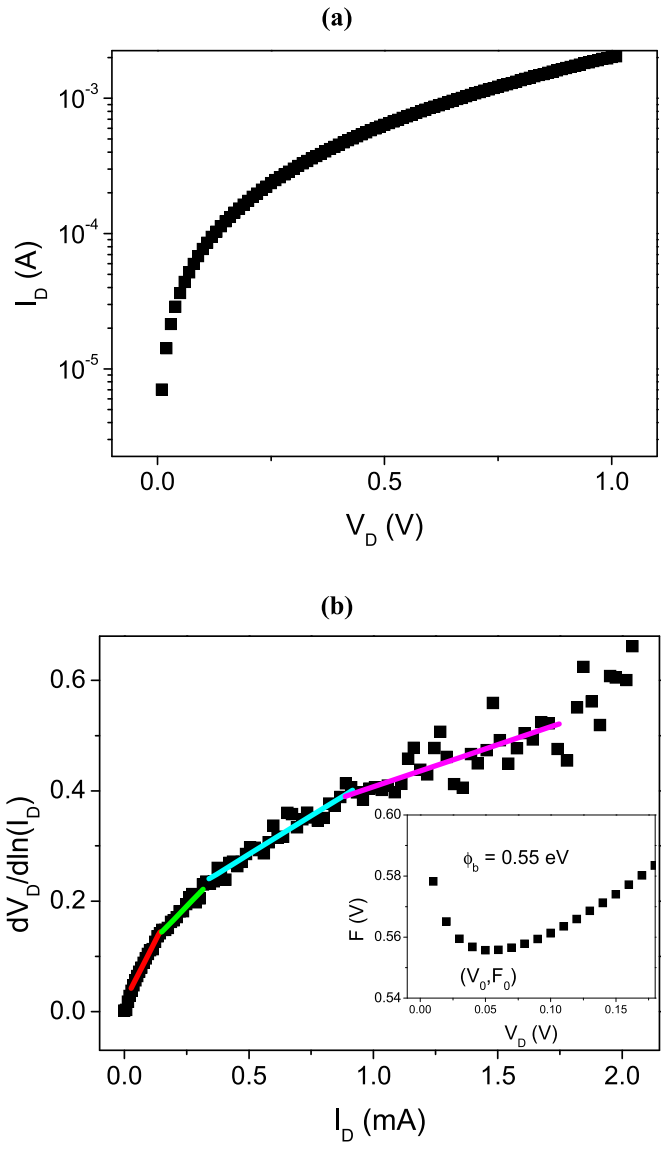

Figure 5. Experimental characteristics for ZnO based SBD. (a) semilogarithmic $I-V$ plot. (b) $dV_D/dln(I_D)$ versus I_D plot, four quasi-linear regions are depicted by the straight lines. In the inset the corresponding Norde function is shown.

Table 3. Summary of the ideality factor obtained from the different regions depicted in figure 5. For comparison the bias range used is shown.

Region	y-axis intercept	η	Voltage Range(V)
1	0.01867	0.72	0.04–0.17
2	0.0744	2.8	0.17–0.31
3	0.1488	5.7	0.33–0.63
4	0.2645	10.2	0.62–0.92

From (1), the logarithmic diode current at $V_D \gg kT/q$ will be rewritten as:

$$ln(I_D) = ln(AA^*T^2) - \frac{q}{kT}\phi_b(V_D) + \frac{q}{kT}\left(\frac{V_D}{\eta(V_D)}\right) \tag{9}$$

Therefore, its derivative respect V_D will be:

$$\frac{dln(I_D)}{dV_D} = -\frac{q}{kT}\cdot\frac{d\phi_b(V_D)}{dV_D} + \frac{q}{kT}\cdot\frac{d}{dV_D}\left[\frac{V_D}{\eta(V_D)}\right] \tag{10}$$

Considering the series resistance and (3), the derivative becomes:

$$\frac{dln(I_D)}{dV_D} = -\frac{q}{kT}\cdot\frac{d\phi_b(V_D)}{dV_D} + \frac{q}{kT}\cdot\frac{d}{dV_D}\left[\frac{V_D - I_D R_S(V_D)}{\eta(V_D)}\right] \tag{11}$$

In order to be able to solve (10) and (11) it is necessary to know the mathematical dependence of the diode parameters with V_D. Also, in these equations the dependency of the three diode parameters is included. Nevertheless, if only one parameter becomes bias dependent, the extraction methods will not be valid anymore, since the corresponding derivative of the bias dependent parameter must be included.

5. Experimental *I–V* characteristics

The extraction procedures were applied to experimental diode characteristics of ZnO nanoparticles-based diodes fabricated as indicated in [26]. Figures 5(a) and (b) show, respectively, the measured semilogarithmic *I–V* plot in the bias range from 0 to 1 V, and the $dV_D/dln(I_D)$ versus I_D, plot as well as the Norde function plot versus V_D in the inset of figure 5(b).

As observed, the minimum of the *F* function is well-defined, and a barrier height value of about 0.55 eV can be estimated. However, similar behaviour than the shown in figure 3(a) and (b) is observed in the experimental measured diode, the semilogarithmic *I–V* plot does not exhibit a linear region and therefore the idealized extraction process cannot be applied. The $dV_D/dln(I_D)$ versus current plot, neither exhibits a linear behaviour, which implies that (4) is not valid. In a similar form than figure 4(c), different quasi-linear regions could be identified within a limited bias range, if Cheung method is applied at each region depicted in figure 5(b), different ideality factor values would be obtained as table 3 summarizes, with the corresponding bias range. It is worth noting that the low value of the ϕ_b reinforce assumption that extraction becomes more challenging for devices with low barrier and large series resistance.

Therefore, the reliability of the extraction process cannot be assured because the curve bending exhibited in figure 5(b), clearly involves the presence of some extra bias dependent phenomenon not considered in the extraction methodologies.

6. Conclusions

Schottky Barrier Diode current—voltage characteristics, considering constant as well as considering bias dependent series resistance were numerically calculated. Overall results indicate that Cheung and Norde methods can accurately estimate the diode parameters for devices that exhibit bias independent parameters, even for relatively large series resistance. On the contrary, the studied extraction methods fail when the *I–V* characteristics includes bias dependent series resistance. As a consequence, a fictitious increment on the estimated value of the ideality factor is produced, and the extracted value will change depending on the bias used to perform the extraction. The low values on the metal-semiconductor barrier height, usually reported for nanostructured SBD, implies a more challenging condition to properly apply the analysed extraction methods.

Data availability statement

The data cannot be made publicly available upon publication because no suitable repository exists for hosting data in this field of study. The data that support the findings of this study are available upon reasonable request from the authors.

References

[1] Zhang F *et al* 2024 *IEEE Trans. Electron Devices* **71** 3560
[2] Basov M 2021 *Sens. Actuators A* **331** 112930
[3] Hu Y, Zhou J, Yeh P-H, Li Z, Wei T-Y and Wang Z L 2010 *Adv. Mater.* **22** 3327
[4] Chakraborty M, Kadir E S, Pradhan M, Kangsabanik M, De S and Gayen R N 2024 *Opt. Mater.* **148** 114976
[5] Ali A, Lee J, Kim K, Oh H and Yi G-C 2024 *Adv. Healthcare Mater.* **13** 2304140
[6] Özmenteş R, Jamil N Y, Al Taan L M and Al Abbas J 2024 *Semiconductors* **58** 631
[7] Yilmaz M, Cirak B B, Aydogan S, Grilli M L and Biber M 2018 *Superlattices Microstruct.* **113** 310e318
[8] Mahmoud W E, Al-Ghamdi A A, Shirbeeny W, Al-Hazmi F S and Khan S A 2013 *Superlattices Microstruct.* **63** 162
[9] Lee S-Y, Jang C-O, Hyung J-H, Kim T-H and Lee S-K 2008 *Physica E* **40** 3092
[10] Ali G M 2020 *J. Alloys Compd.* **831** 154859
[11] Ali G M, Khalid A K and Swadi S M 2020 *J. Semiconduct.* **41** 02103
[12] Mwankemwa B S, Legodi M J, Mlambo M, Nel J M and Diale M 2017 *Superlattices Microstruct.* **107** 163e171
[13] Faraz S M, Tajwara Z, Wahab Q U, Ulyashinc A and Yakimova R 2022 *Acta Phys. Pol. A* **141** 99

[14] Daniel T T, Yadav V K S, Natu G and Paily R 2021 *IEEE Electron Device Lett.* **42** 1212
[15] Chan Y C, Yu J and Ho D 2018 *Appl. Surf. Sci.* **443** 506
[16] Varma T, Periasamy C and Boolchandani D 2017 *Superlattices Microstruct.* **112** 151e163
[17] Singh B K and Tripathi S 2015 *Superlattices Microstruct.* **85** 697
[18] Armoot S T and Ali G M 2022 *Proc. IEEE 22nd Int. Conf. on Nanotechnology (NANO)* 211–2014 (https://doi.org/10.1109/NANO54668.2022.9928680)
[19] Gayen R N, Paul R and Biswas S 2020 *Appl. Surf. Sci.* **533** 147149
[20] Ranaa V S, Rajput J K, Pathak T K and Purohit L P 2019 *Thin Solid Films* **679** 79
[21] Caglar Y, Caglar M and Ilican S 2018 *Optik* **164** 424
[22] Chaitra U, Ali A V M, Mahesha M G, Kompa A, Kekuda D and Rao K M 2021 *Superlattices Microstruct.* **155** 106903
[23] Zheng K O, Rosli N, Rashid M M M and Halim M M 2023 *Physica B* **648** 414425
[24] Zhang X A, Zhai J X, Yu X K, Ding L H and Zhang W F 2013 *Thin Solid Films* **548** 623
[25] Zhang X, Hai F, Zhang T, Jia C, Sun X, Ding L and Zhang W 2012 *Microelectron. Eng.* **93** 5
[26] Tinoco J C, Hernandez S A, Olvera M L, Estrada M, Garcia R and Martinez-Lopez A G 2022 *Micromachines* **13** 800
[27] Park H K and Choi J 2018 *Adv. Electron. Mater.* **4** 1700317
[28] Saha B, Sarkar K, Bera A, Deb K and Thapa R 2017 *Appl. Surf. Sci.* **418** 328
[29] Dey A, Middya S, Jana R, Das M, Datta J, Layek A and Ray P P 2016 *J. Mater. Sci.: Mater. Electron.* **27** 6325
[30] Al-Ghamdi A A, Al-Ghamdi A A, Al-Hartomy O A, Nawar A M, El-Gazzar E, El-Tantawy F and Yakuphanoglu F 2013 *J. Sol.-Gel Sci. Technol.* **67** 368
[31] Kim J, Yun J-H, Kim C H, Park Y C, Woo J Y, Park J, Lee J-H, Junsin Y and Han C-S 2010 *Nanotechnology* **21** 115205
[32] Cheung S K and Cheung N W 1989 *Appl. Phys. Lett.* **49** 85
[33] Norde H A 1979 *J. Appl. Phys.* **50** 5052
[34] Ortiz-Conde A and García-Sánchez J 2018 *Solid-State Electron.* **144** 33
[35] Olikh O Y 2015 *J. Appl. Phys.* **118** 024502